Danmarks Tekniske Universitet DTU

Robust Design of Products and Mechanisms
Poster Appendix

Authors

Peter Selzer Rasmussen - s183637
Morten Deurell - s206073
Tobias Canger Lund - s214365
Oscar Max Hagemann - s214356
Oscar Lowe - s242099
Juliette Claire Therese Auburtin - s243581

April 11, 2025

Contents

Workload

1 Concept

After exploring a few different ideas that quickly ballooned in terms of functionality requirements, we settled on a two player flipper machine as illustrated in Figure 1 below:

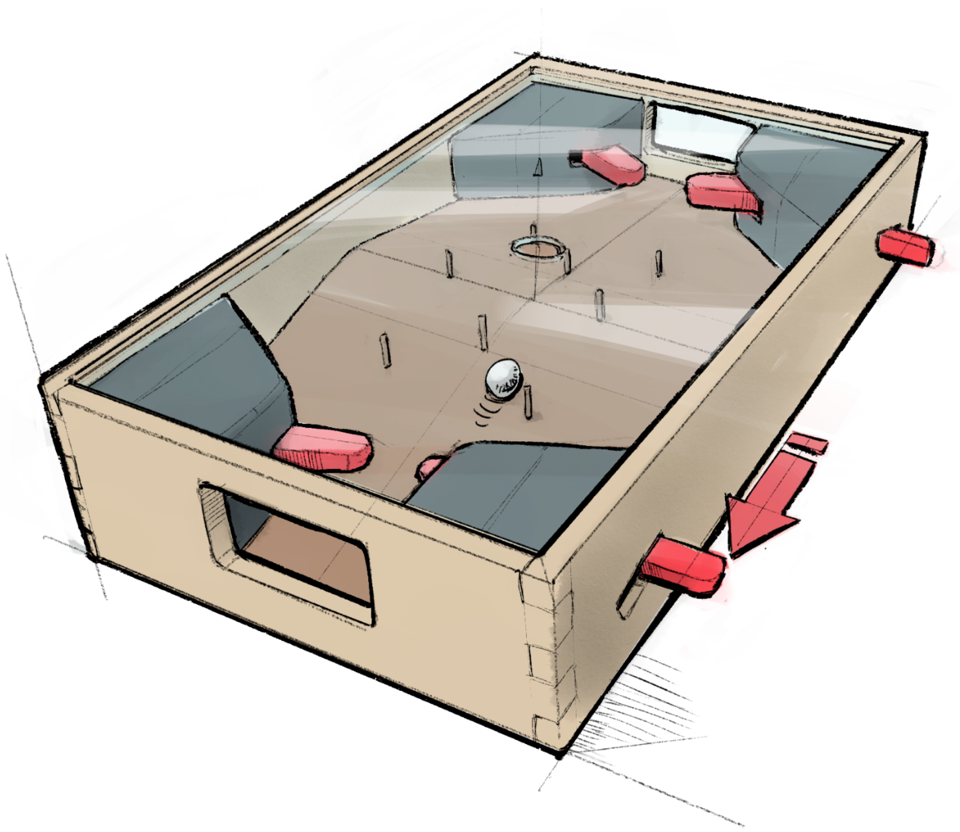

Figure 1: Two player flipper machine

The two players sit at either end of the box, that has a floor that is highest in the middle, and gently slopes down to either side. The game begins when the ball is dropped through the hole in the acrylic covering in the middle of the box. Newton takes over, and the two players will use controls on both sides to have the flippers smack the ball away from their own goal. The flippers should be far enough apart at a resting position, to allow the ball to pass between. The turn ends when the losing player has to pluck out the ball from behind their own flippers and initiate a new round, by dropping the ball through the central hole again. Pins are placed in the floor to add some of the classic pinball randomness, and also to avoid that a dropped ball goes directly into a goal after being dropped.

2 Mechanism Constraints and Tolerances

2.1 Peter's concept

This concept is inspired by the classic flipper machines, where the user bashes a button on the side of the machine to actuate the flipper rotation. This has been sketched in figure 2 as a rack & pinion mechanism that converts a translational movement to a rotational movement.

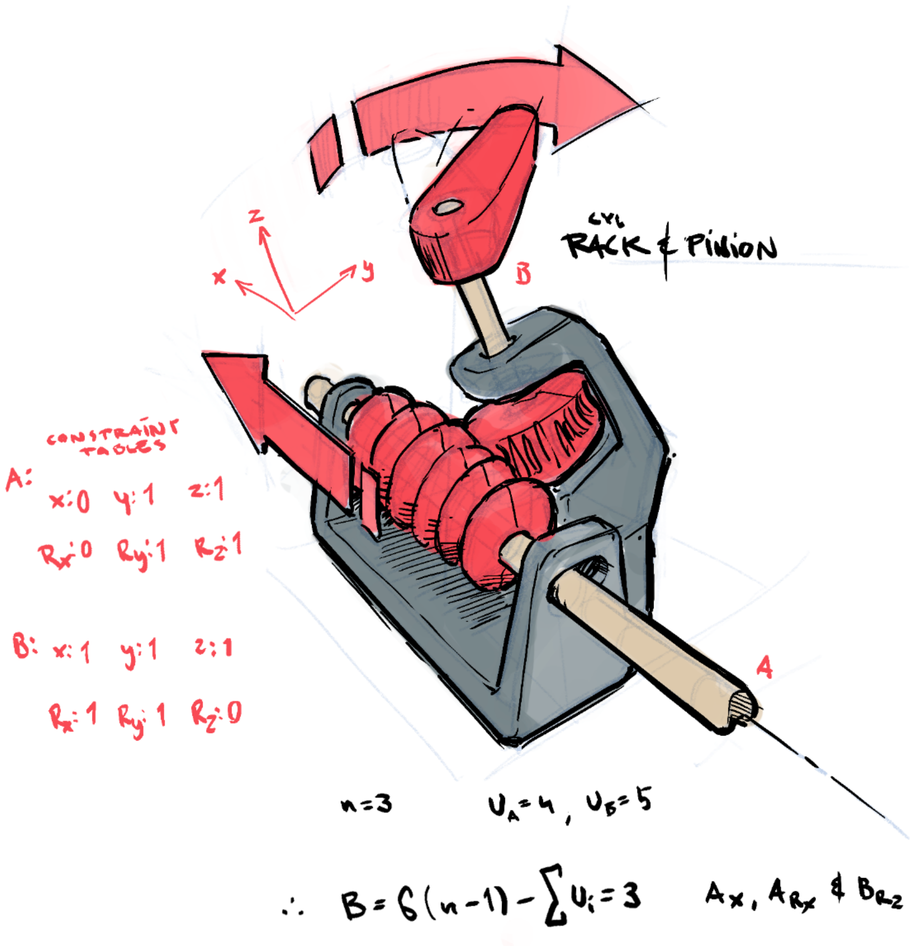

Figure 2: Mechanism sketch, rack & pinion

The rack has been made cylindrical to allow it, along with the rod, to rotate freely without compromising the functionality. This means that the assembly would have one more degree of freedom than is essentially required, but in a way that would not interfere with the functionality as far as we could tell. However, the parts turned out to be tricky to print without infill between the teeth on the rotationally symmertrical rack. Which along with other complexity issues got us on better thoughts, as you will see in the following sections.

2.2 Morten's concept

The developed flipper mechanism is a classic rotational link: motion is transferred between three components, each rotating around its own axis. Early on, I explored references like "507 Mechanical Movements" but found no alternative more suitable for the project goals.

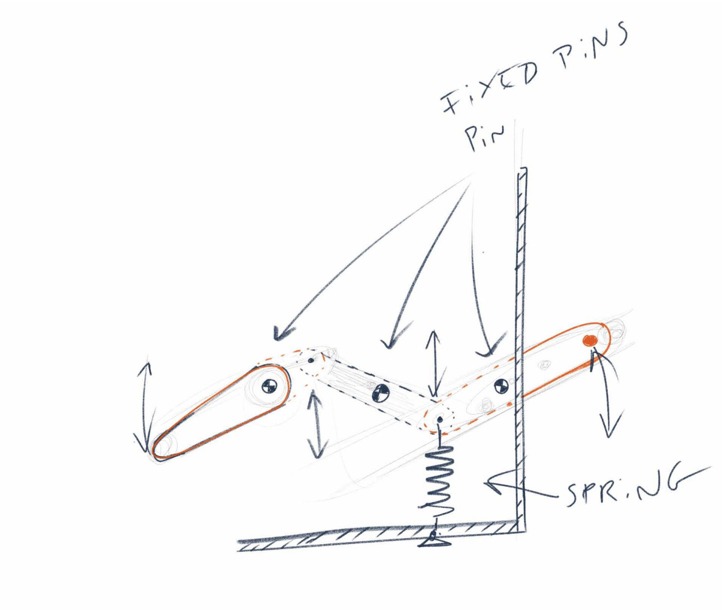

Figure 3: flipper-sketch

The general dimensions of the mechanism were defined primarily by three constraints: the size of the PMMA sheets, the working area of the laser cutter, and the 23 mm ball used in the game. Within these limits, the flipper system was proportioned to ensure that the handle could protrude from the shell, and that the flippers extended nearly to the centerline of the playing field for effective gameplay.

The transfer pin - the central moving part - was designed as a symmetric element, both to simplify force transmission and to match the 50mm axis spacing between handle and flipper. This symmetry also made fabrication and alignment easier during assembly.

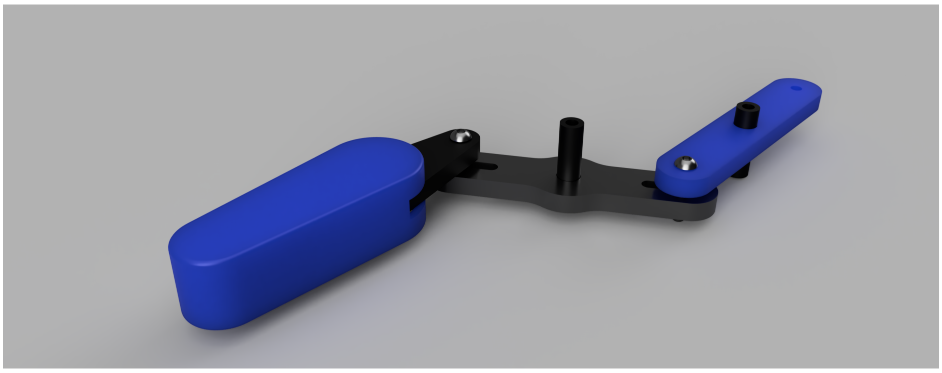

Figure 4: Flipper rendering

From the beginning, it was clear that the mechanism tolerated relatively large dimensional variation. Most tolerances were therefore deliberately generous - especially for the flipper and handle openings in the shell. The only semi-tight fit was between the laser-cut flipper arm and the 3D-printed flipper cover.

The design was iterated several times. A few early prototypes were accidentally over-constrained, which highlighted the importance of keeping the transfer pin joints as slots, not holes. The final mechanism works well and is robust, though the spring was selected intuitively, without formal calculation.

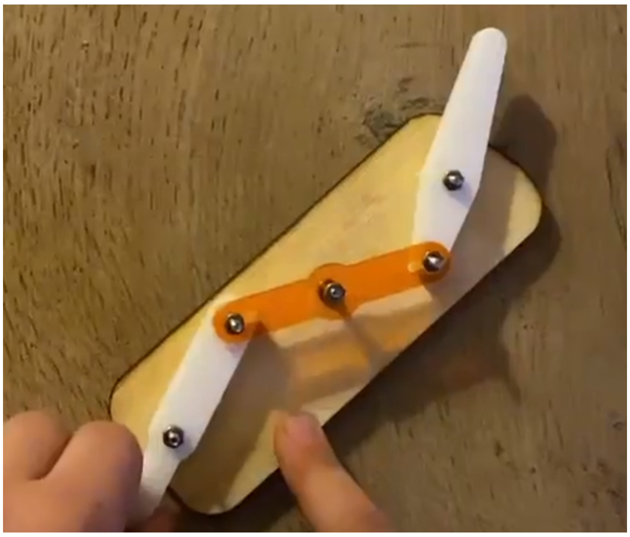

Figure 5: Enter Caption

For the ball feeder, constraints were also considered: a pin joint and a slot joint anchor the component while allowing a small degree of freedom to prevent over-constraint. Another assembly-related insight was making the flipper axle removable, so spacers could be added later. Earlier versions had spacers fixed to the shell, which blocked handle assembly.

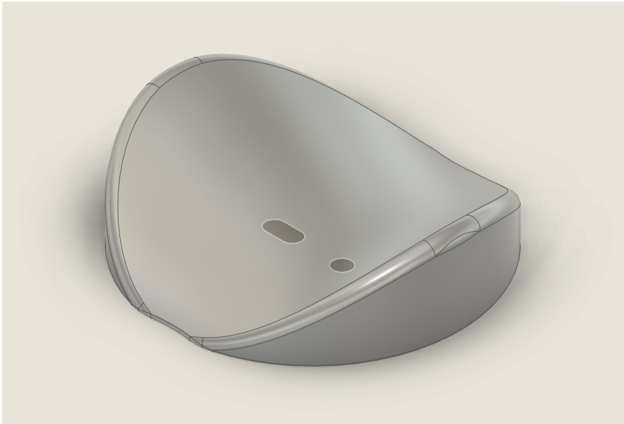

Figure 6: CAD Ball feeder

Finally, the small obstacles on the playing field were fixed with a single bolt each. While visually effective, this solution made them rotate easily - they couldnât function as nuts, and future iterations would require better fixation.

2.3 Juliette's concept

2.3.1 Initial concept

The initial concept was converting a translation from a pushing-button to a rotation of the flipper. The allowed rotation of the flipper is $-45deg$ to $+45deg$. The concept is illustrated in Figure 7.

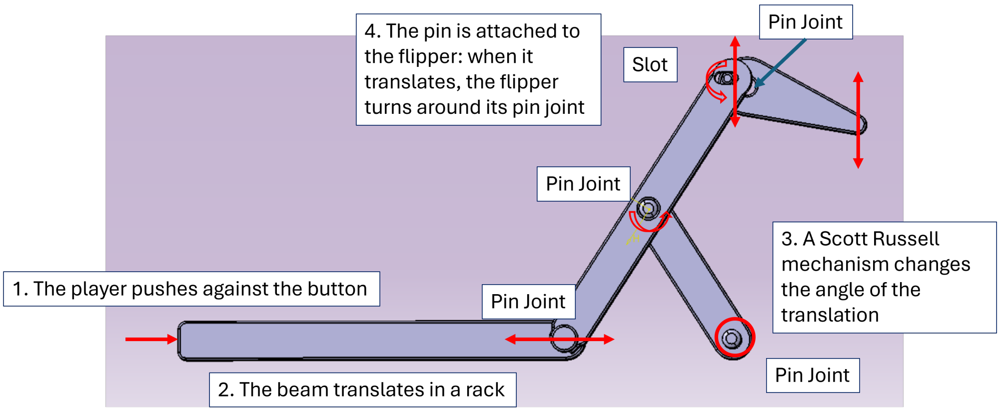

Figure 7: Initial Juliette's mechanism

The critical part is the joint between the Scott Russel mechanism and the flipper: we want to convert a translation into a rotation and we want to limit variations of rotational speed of the flipper. Hence, the rack is short and little variations can have high impacts on the mechanism, which is not robust.

2.3.2 Upgrade and analysis

Upgrades to the initial mechanism include ergonomic improvements to the actuator (Figure 8, implementation of spring mounting surfaces for fast retraction, in-built adjustability (as seen in Figure 10 and stability and longevity improvements thanks to the use of several metal components. It is important to mention that the kinematics of this iterated version remain unchanged.

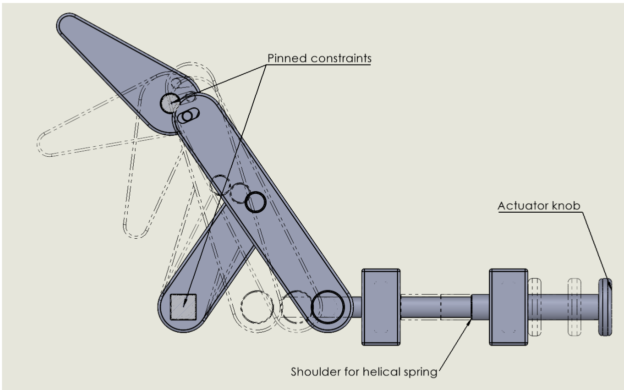

Figure 8: Upgraded mechanism showing full range of movement

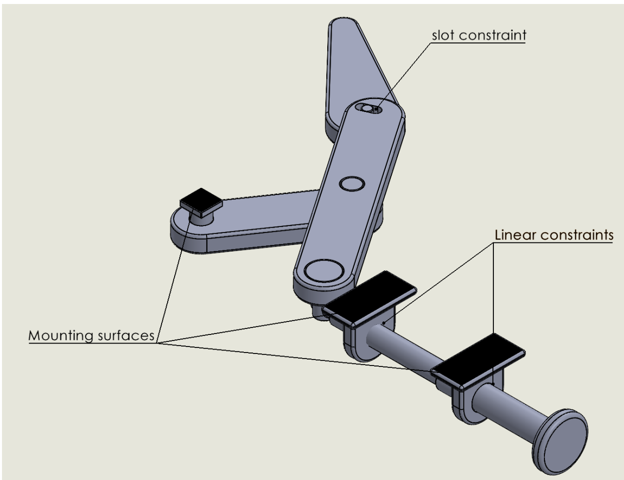

Figure 9: Alernate view of the mechanism

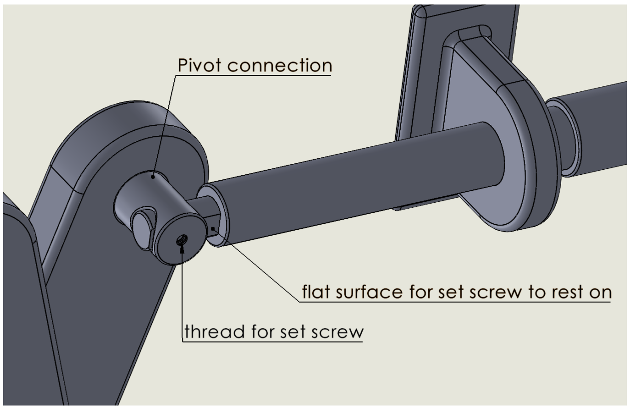

Figure 10: Close-up of the metal pivot connection component

The Gruebler-Kutzbach criterion for planar mechanisms is given by:

$$B = 3(n-1) - \sum U_i - \sum F_{id} \tag{1}$$

Where:

- B = Mobility (number of degrees of freedom or motors required)
- n = Number of links/bodies (including the fixed ground)
- U_i = Number of constraints (unfreedoms) at joint i
- F_{id} = Number of identical degrees of freedom constrained more than once (redundant constraints)

Applied to this mechanism: The mechanism features 4 links, each pin joint constrains movement in 2 directions (x and y), furthermore, the top-most joint is constrained in the y-direction, and the slot allows for movement in one direction only as well as a rotation, therefore presenting one constraint. This makes for a total of 8 constraints throughout the joints, and no identical degrees of freedom.

$$M = 3(4-1) - 8 = 1 \tag{2}$$

The full motion of the mechanism is dependent on one input from the user, through depressing the actuator.

3 Interface and Part Design

3.1 Interface Constraints

Ambiguities

An interface is considered ambiguous if a variation of the designs parameters can change the interfaces and constraints of the design. By identifying and resolving potential ambiguities, we ensure that a part is manufactured and assembled correctly and consistently, reducing the risk of errors and improving functional reliability.

In the case of our mechanism, we use the transfer pin (The blue part in Figure 5) as our starting point. The elongated slots in each end lock the Y-direction. A pin going through the middle of the transfer pin locks the X-direction and a bolt locks the Z-direction.
The bolt also locks the Rx- and Ry rotation.

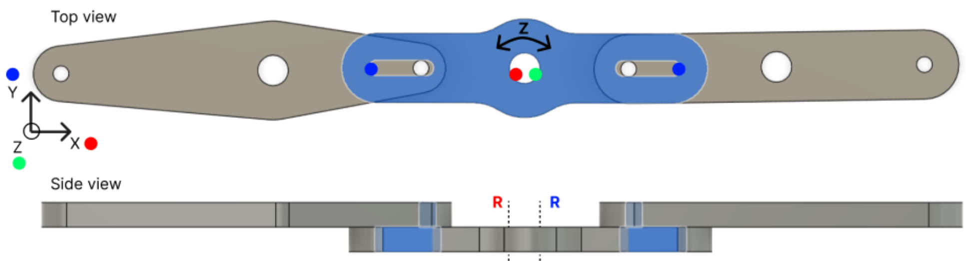

Intended constraints		
X 1	Y 1	Z 1
Rx 1	Ry 1	Rz 0
Actual constraints		
X 1	Y 1	Z 1
Rx 1	Ry 1	Rz 0

Figure 11: Ambiguities

Since the intended and actual constraints are identical, then in theory, there shouldn't be any ambiguities.

Location schemes

Location schemes define how the features of a part like holes, slots, and edges are referenced and dimensioned relative to fixed datums. This ensures accurate and repeatable manufacturing, inspection, and assembly.

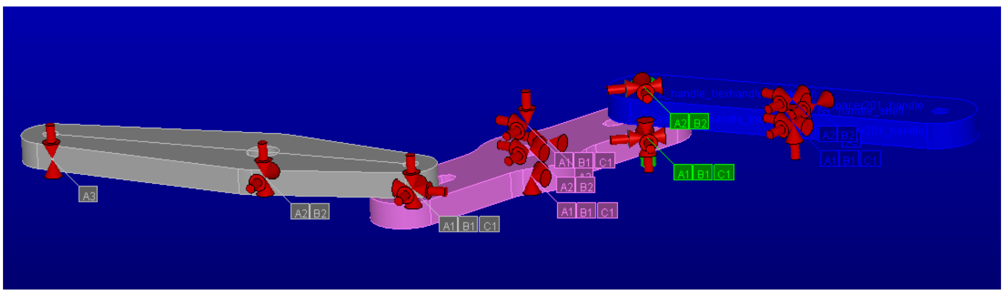

Figure 12: Location schemes of the RD&T model of Section 4.2

3.2 Measurement of prints

3.3 RD&T Analysis

The whole RD&T model is described in Section 4.2. Here, we reduce the study to the bare mechanism composed of three parts: the handle, the transfer pin, and the flipper.

We want to verify that the axes of the hexagonal screws between the handle and the transfer pin as well as the transfer pin and the flipper are confounded, so that the transmission of movement is enabled. Thus, we need to compare the parallelism between the axes and the distance between the contacting points.

The coaxiality is studied when the flipper is inclined by $30deg$ compared to the horizontal. This case is more difficult to study using tolerance stacking and suffers from the accumulation of variations at the furthest point from the rotational axis.

In RD&T, we created the axes of those parts using points centered on holes. This created four axes in total, two pairs of two, as illustrated in Figure 13. The distance between the points is evaluated in the plane XY since the vertical distance does not raise any threat to coaxiality.

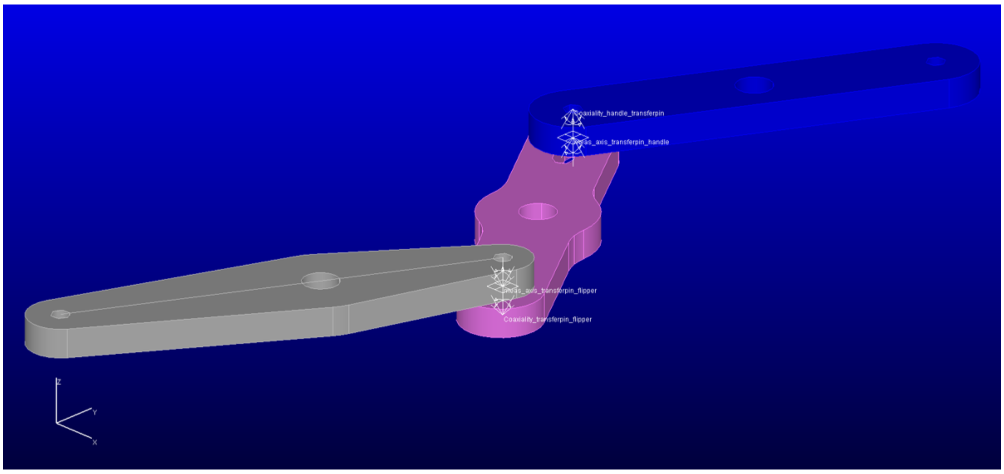

Figure 13: Measures in RD&T of the coaxiality of two pairs of two axes

The measures are reported in Table 1. We considered the values in 95% of cases, meaning that the variation is equal to $\pm\sigma$.

	Axis angle (in degrees)	Point distance (in mm)
Handle to transfer pin	0.617 ± 0.662	1.67 ± 2.10
Transfer pin to flipper	0.703 ± 0.758	1.22 ± 1.816

Table 1: Measures from RD&T regarding the axis transfering the rotational movement

The conclusion of those measures is that the parallelism between axes should be verified, since the angle difference is really small compared to the height of the parts ($5mm$).

Nevertheless, the contact points could be positioned too far away from each other in the plane XY in both cases. The diameter margin between the parts is only $1mm$.

According to the sensitivity matrix of RD&T, both parts of each pin joint have the same amount of impact on those variations. Laser-cutting is supposedly far more precise than 3D-printing. If the theoretical tolerancing values for the laser-cutting are not overestimated, we should then increase the diameter margin of both parts by approximately $2mm$ to meet the functional requirements.

3.4 GPS Tolerances

Printer Type	Prusa i3 Mk3
Print Material	PLA
Relevant Print Settings	Brimless, grid pattern infill (15%), 0.4mm nozzle diameter, 0.15mm layer height, 45mm/s printing speed

Table 2: Printer Information

	Dimension 1			Dimension 2			Dimension 3	
Description	Nominal	Averaged measurement	Description	Nominal	Averaged measurement	Description	Nominal	Averaged measurement
Depth of pinhole	6	5.9	Diameter of pinhole	3.2	3.2	Height of object	18.1	18.05

Table 3: Measured dimensions (all values in mm)

The feature of interest whilst designing the flipper shell is the pin-hole located nearer the wide end of the body. It's function is to keep the flipper arm constrained in x and y directions, whilst allowing for rotation, hence actioning the flipper when there is an input from the user. The specific dimensions we'll be looking at are the diameter and depth of this hole. An equally important feature of the part is it's overall height, this allows for centering within the mechanism and makes for an effortless transfer of movement from input to output. Tolerances equally considered are displayed in Figure 14 according to the GPS symbol language. Results for the carried out measurments show an overall tendancy to print features undersize, this is in part due to thermal contraction - the shrinkage of print layers once cooled. Some high end printers feature control loops to attenuate this phenomenon, known as thermal compensation, although according to Prusa's specifications for the MK3 [?], the only feature related to temperature control is a "Thermal model protection", which terminates a print in the case of excessive temperatures. Notice this negative deviation in dimensions follows the trend of undersize part dimensions found in this year's 3D-print statistics file, regardless of feature type or printer utilised. For this reason, rather than troubleshooting prints (modifying input parameters and designed dimensions - an iterative and oftentimes timely procedure), our team opted to change our manufacturing methods for vital parts. We found that laser cutting our joints to size made for more suitable tolerance values, using analogue measuring methods (vernier calipers), we were unable to find any discernable deviation from nominal value for pins and pin-holes manufactured this way. A slight redesign was therefore necessary in order to interface two laser-cut parts (a pin extruded from the flipper and a hole built into the base of the assembly), leading to a far better joint operation. The decreased surface roughness also aided in smooth rotation thanks to a lower friction coefficient between the two parts.

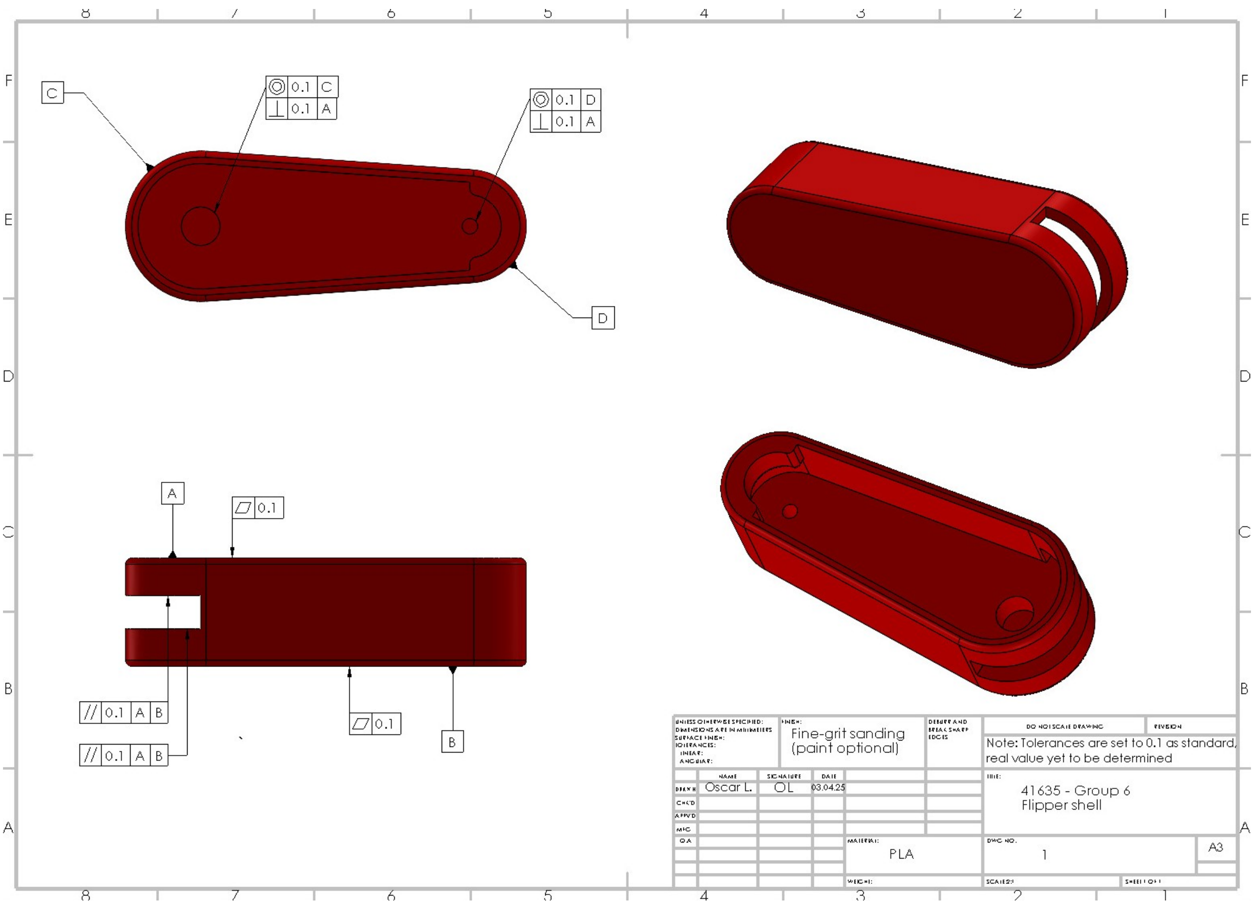

Figure 14: GPS labeling (all values are symbolic)

4 Final Mechanism Solution

Morten

4.1 Tolerance Specification and Stack-Up Analysis

The tolerance chain has been developed in accordance with the ISO 268/2768 standard. There have been used H7 for tight holes (shaft attachements), and H11 for looser fits (sliding hole and edge holes).
The following document are the calculations made to create the RSS and the tolerance graph:

$with(Gym)$:
RSS calculations:

All our tolerances:
$T_1 := 0.1$:
$T_2 := 0.015$:
$T_3 := 0.15$:
$T_4 := 0.1$:
$T_5 := 0.015$:
$T_6 := 0.05$:
$T_7 := 0.05$:
$T_8 := 0.1$:
$T_9 := 0.015$:
$T_{10} := 0.15$:
$T_{11} := 0.1$:
$T_{12} := 0.1$:
$T_{13} := 0.1$:
$T_{14} := 0.1$:
$T_{15} := 0.1$:
$T_{16} := 0.1$:
$T_{17} := 0.15$:

$$RSS := \left(T_1^2 + T_2^2 + T_3^2 + T_4^2 + T_5^2 + T_6^2 + T_7^2 + T_8^2 + T_9^2 + T_{10}^2 + T_{11}^2 + T_{12}^2 + T_{13}^2 + T_{14}^2 + T_{15}^2 + T_{16}^2 + T_{17}^2\right)^{1/2}$$

$$RSS := 0.4039492542 \quad \textbf{(1)}$$

Worst case scenario:

$$WC := T_1 + T_2 + T_3 + T_4 + T_5 + T_6 + T_7 + T_8 + T_9 + T_{10} + T_{11} + T_{12} + T_{13} + T_{14} + T_{15} + T_{16} + T_{17}$$

$$WC := 1.495 \quad \textbf{(2)}$$

The mean:

$$\mu := \frac{T_1 + T_2 + T_3 + T_4 + T_5 + T_6 + T_7 + T_8 + T_9 + T_{10} + T_{11} + T_{12} + T_{13} + T_{14} + T_{15} + T_{16} + T_{17}}{17}$$

$$\mu := 0.08794117645 \quad \textbf{(3)}$$

The spread/variance/standard deviation:

$$\sigma := \frac{1}{17}\left(\left(T_1 - \mu\right)^2 + \left(T_2 - \mu\right)^2 + \left(T_3 - \mu\right)^2 + \left(T_4 - \mu\right)^2 + \left(T_5 - \mu\right)^2 + \left(T_6 - \mu\right)^2 + \left(T_7 - \mu\right)^2 +\right.$$

$$\left(T_8-\mu\right)^2+\left(T_9-\mu\right)^2+\left(T_{10}-\mu\right)^2+\left(T_{11}-\mu\right)^2+\left(T_{12}-\mu\right)^2+\left(T_{13}-\mu\right)^2+\left(T_{14}-\mu\right)^2+\left(T_{15}-\mu\right)^2+\left(T_{16}-\mu\right)^2+\left(T_{17}-\mu\right)^2\Big)$$

$$\sigma := 0.001864878894 \tag{4}$$

The spread is rooted, because it was not squared in the previous step:

$$f(x) := \frac{1}{\sqrt{\sigma}\cdot\sqrt{2\cdot \mathrm{Pi}}}\cdot \mathrm{e}^{\frac{-(x-\mu)^2}{2\cdot\sigma}}$$

$$f := x \mapsto \frac{\mathrm{e}^{-\frac{(x-\mu)^2}{2\cdot\sigma}}}{\sqrt{\sigma}\cdot\sqrt{2\cdot\pi}} \tag{5}$$

The tolerance graph with cuts at $\mu-3\cdot\sigma, \mu-2\cdot\sigma, \mu+2\cdot\sigma$ and $\mu+3\cdot\sigma$ (the spreads are still rooted)

$$plot\Big(\Big\{f(x), \big[\big[\mu-3\cdot\sqrt{\sigma}, 0\big], \big[\mu-3\cdot\sqrt{\sigma}, 9.5\big]\big], \big[\big[\mu+3\cdot\sqrt{\sigma}, 0\big], \big[\mu+3\cdot\sqrt{\sigma}, 9.5\big]\big], \big[\big[\mu-2\cdot\sqrt{\sigma}, 0\big], \big[\mu-2\cdot\sqrt{\sigma}, 9.5\big]\big], \big[\big[\mu+2\cdot\sqrt{\sigma}, 0\big], \big[\mu+2\cdot\sqrt{\sigma}, 9.5\big]\big]\Big\}, x=-0.1..0.3\Big)$$

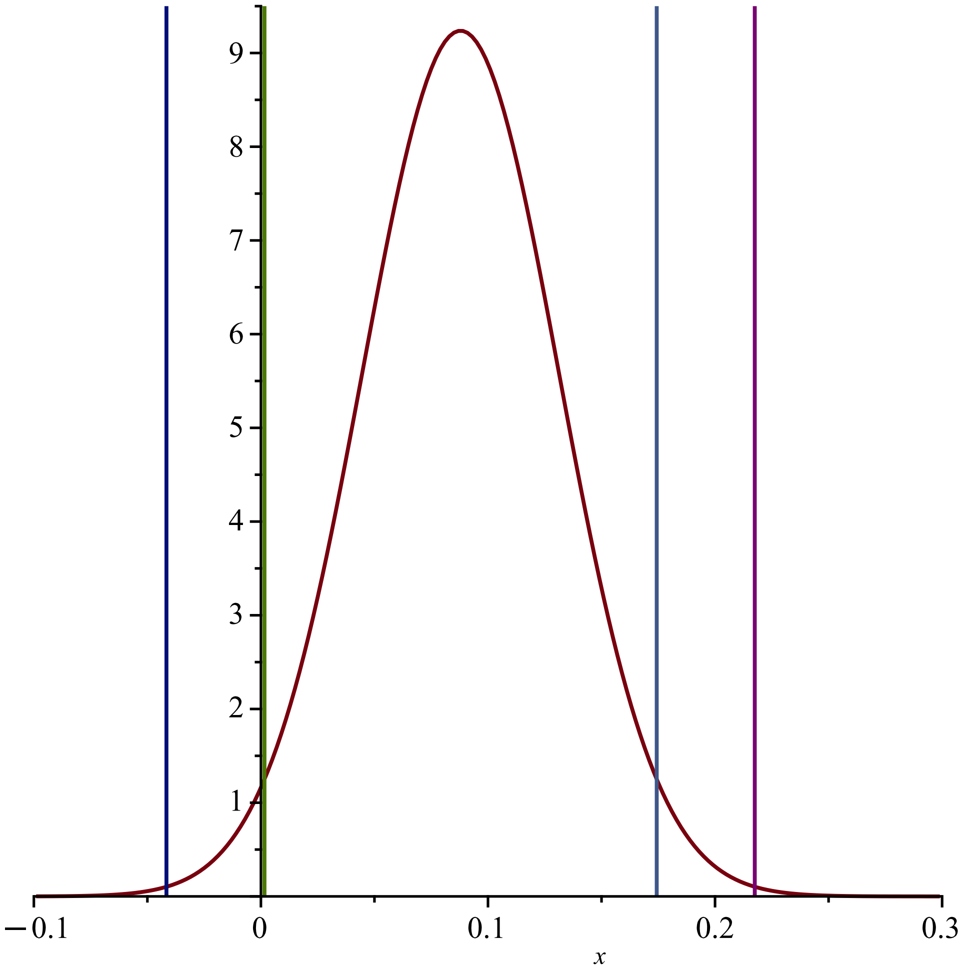

4.2 Sensitivity Analysis

4.2.1 Nomenclature

The whole game is reduced to a functional unit, which consists of the enclosure of the mechanism, its shell, its fixative parts, and the mechanism itself. The exact names given to the different parts of this functional unit are written on Figures 15, 16, and 17.

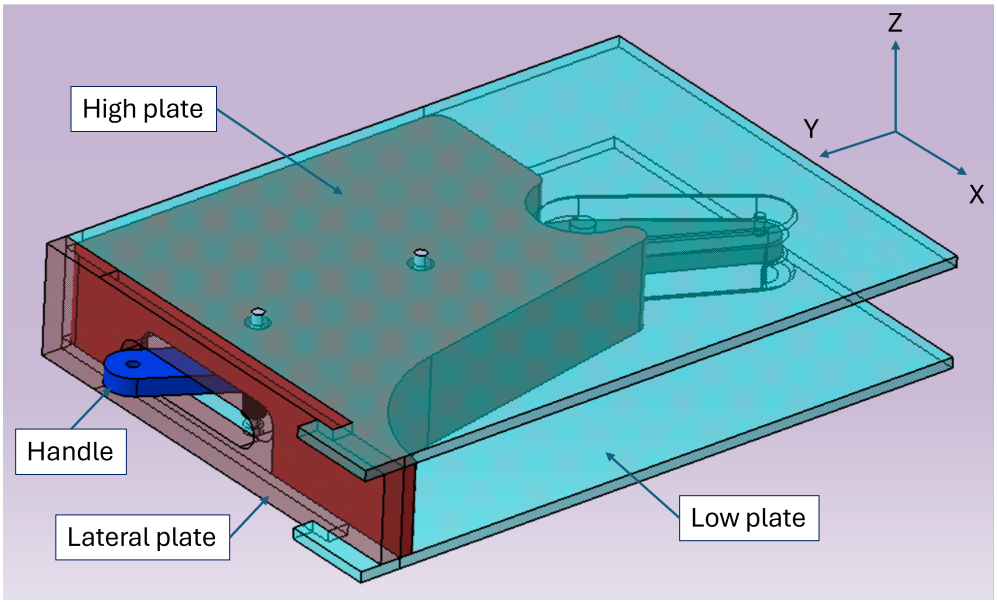

Figure 15: Names of the parts on the CAD model, including the upper PLA plate

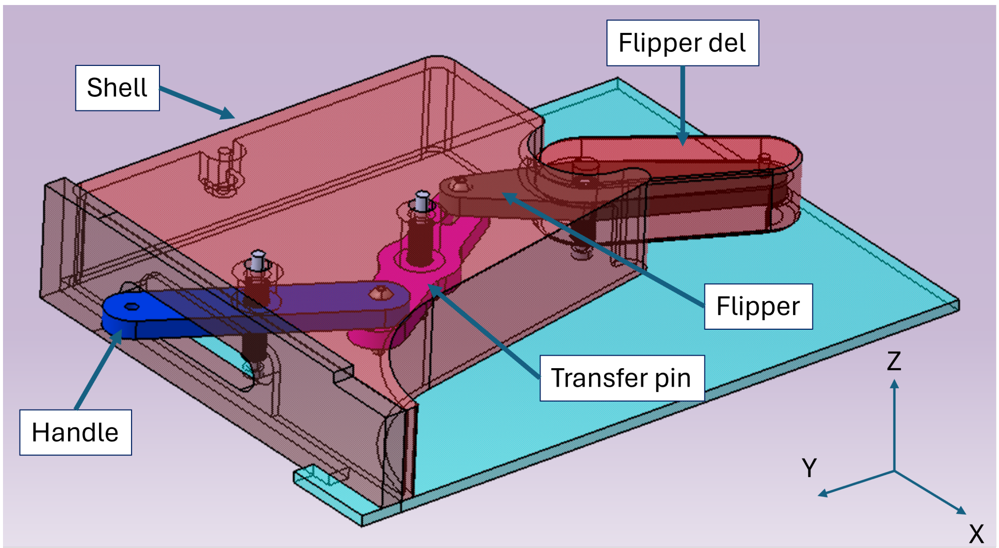

Figure 16: Names of the parts on the CAD model, without the upper PLA plate

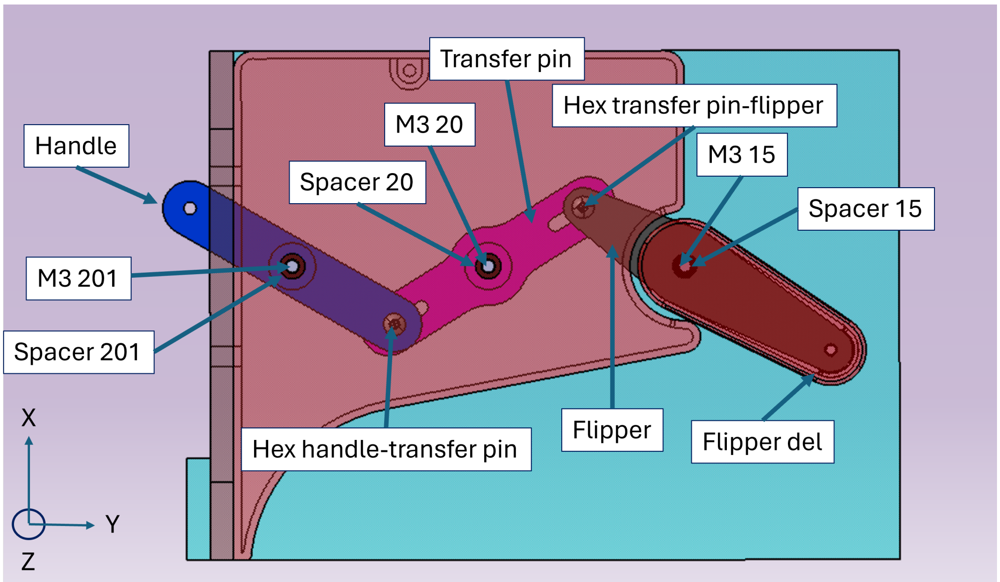

Figure 17: Names given to the parts of the mechanism in the XY vue, which corresponds to the mechanism itself without its container

4.2.2 Aim of the Sensitivity Analysis

The software RD&T has been used to study the sensitivity of the mechanism. Since the CAD model was imported on CATIA V5, we were able to use *.wrl* files to directly preserve the relative positioning of parts and use extensively the "Copy Target" command. Thus, the part being positioned had initially no point, and they were copied from the target, i.e. the positioning parts.

The mechanism normally moves through its use. The flipper is supposed to go through $-30deg$ to $+30deg$ compared to the YZ plane. We study the second extreme position +30. The aim is to verify that pin joints between *handle* and *transfer_pin*, as well as *transfer_pin* and *flipper* function correctly, i.e. the coaxiality of the axes between these pieces. The maximum possible angle of the flipper is calculated using the space between *shell* and *flipper_del*. The study is also used to outline lack of robustness in the mechanism regarding positioning between parts.

4.2.3 Hypothesis

We will position all parts relative to *low_plate*, since the whole mechanism is attached to it. In reality, this plate is bent by the *lateral_plate* further away from the functional unit. Thus, *low_plate* and *high_plate* are not parallel.

Nevertheless, the model approximates this situation, since the angle difference is taken by the nuts associated with screws $M320$ and $M3201$ (not on the schematics). Instead of having a plane-plane interaction with *high_plate*, those nuts will be in contact through one point. Furthermore, the angle is small enough to consider the coaxiality of the plates, which is observed in reality.

Since standard pieces from the Skylab were used (screws and washers), we do not know their tolerancing. In this study, we consider them as perfect, or at least having tolerances that are negligible compared to the ones caused by 3D printing and laser cutting.

Regarding laser cutting, we face the same issue. We consider that the thickness of the standard plates is perfect, but the cutting is not. A laser beam being usually $0.1mm$-wide, the tolerancing over cutting has also a range of $0.1mm$. This is an approximation that could be more precise if we knew the specifications of the laser cutting machines.

4.2.4 Tolerancing

Once attached to a part, the positioning points fall in one of these three categories:

- The point is on a laser-cut part. Since the thickness of the plate is considered perfect, only the position of the point on the surface normal to the laser head has a range of variation.
  - If the point is on the edge of the surface, its position can vary on the plane as a whole. Those points have two different linear tolerances, one for each direction of the plane. The range is $0.1mm$ in both cases. See Figure 18.

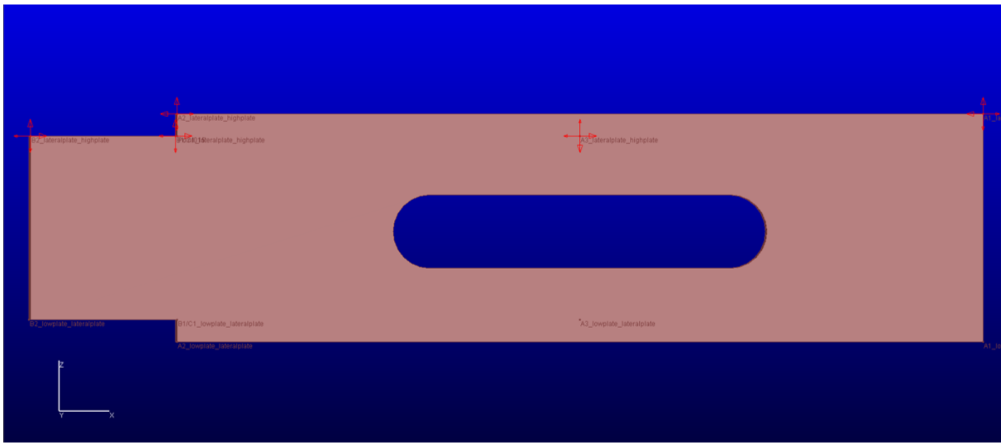

Figure 18: Double linear tolerances on positioning points of the lateral plate, which is laser-cut

  - If the point is on the center of a hole, only the diameter can vary due to the laser head. On the contrary, the position of the center is normally very well located with laser-cutting machines. The chosen tolerance type on those points is "Polar Circular", with a range of $0.1mm$. See Figure 19.

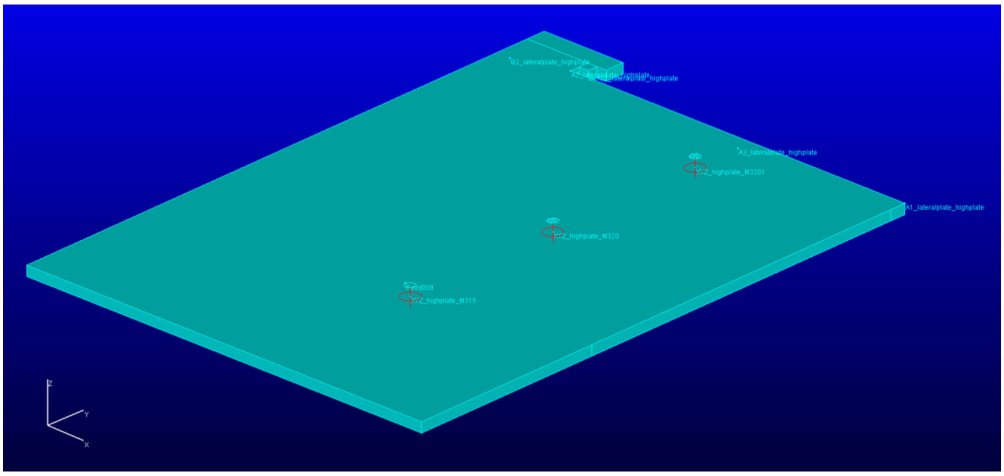

Figure 19: Circular polar tolerances on positioning points of the holes cut in the low plate, which is laser cut

- The point is on a 3D-printed part. We consider that the printers have variations of $0.2mm$ in any direction. Thus, the chosen tolerance type is "Cubic" with a range of $0.2mm$. See Figure 20.

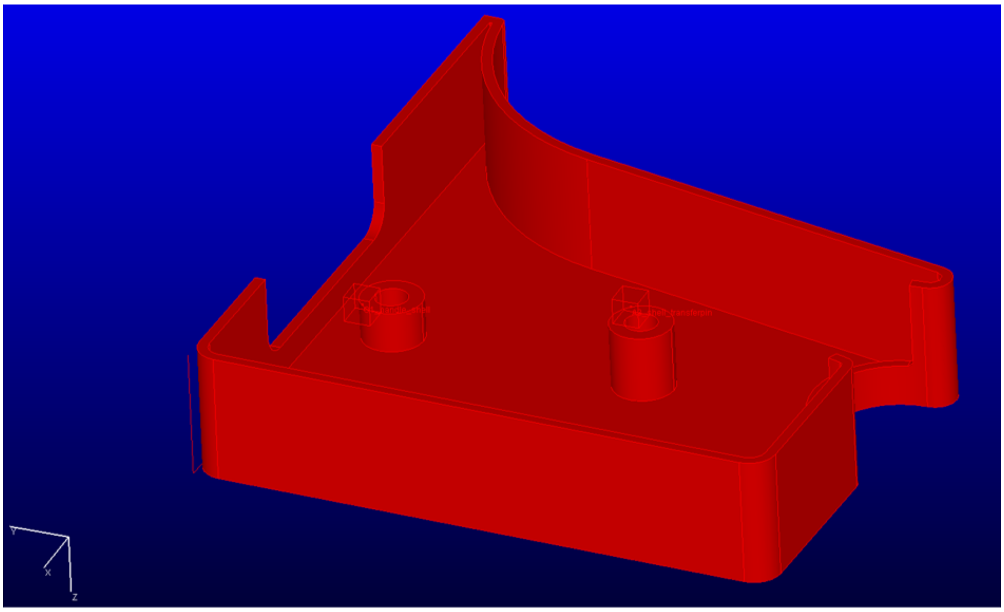

Figure 20: Cubic tolerances on positioning points of the shell, which is 3D-printed

The different parts were manufactured according to Table 4.

4.2.5 Positioning

The ground of the positioning is *low_plate*.

Manufacturing	Laser-cutting	3D-printing	Standard piece
Container	*Shell*	*low_plate*, *high_plate*, *lateral_plate*	$M3201$, $M320$, $M315$
Mechanism itself	*Handle*, *transfer_pin*, *flipper*	*Flipper_del*	$Spacer201$, $spacer20$, $spacer15$, both *hex*

Table 4: Fabrication process of the parts of the mechanism

Container of the mechanism: the so-called container consists of *low_plate*, *lateral_plate*, *high_plate*, $M320$, $M3201$, $M315$ and *shell*.

lateral_plate is positioned relative to *low_plate* with a $3-2-1$ scheme, locking successively R_X, R_Z, T_Y, R_Y, T_Z and T_X. *high_plate* is positioned relative to *lateral_plate* using the same scheme.

The screws $M3201$ and $M320$ are positioned relative to both *low_plate* and *high_plate* following a 2-point scheme. This means that they could theoretically rotate along the Z-axis, but the software virtually locks this degree of freedom. The points are the centers of the laser-cut holes, on the surface closer to the other plate. The screw $M315$ is only positioned through the hole drilled in *low_plate*, also with a 2-point scheme.

Since *shell* is primarily positioned by the holes of the plates, we use a $3-2-1$ positioning locking R_Z, R_Y, T_X, R_X, T_Y and T_Z. The last point is supposed to be chosen on the XY-plane of *shell* in contact with *low_plate*, but the chosen position of this point is arbitrary and can actually impact the whole analysis regarding Z-variations.

The amplitude of variations in these parts with those parameters can be visualized using the MAG tool, as shown in Figure 21.

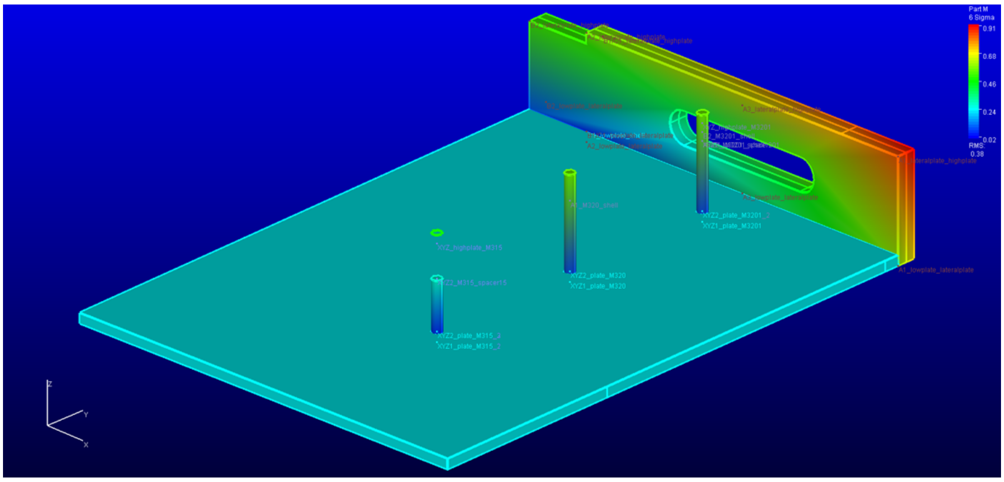

Figure 21: Amplitude of variations accross the contrainer of the mechanism

Mechanism itself: the mechanism consists of *handle*, *transfer_pin*, *flipper*, *flipper_del*, $spacer201$, $spacer20$, $spacer15$, $hex_handle_transferpin$ and $hex_transferpin_flipper$.

The spacers are positioned relative to the screws using a 2-point scheme. The points are affected by the tolerances of *shell* since the spacers sit on it.

Handle, *transfer_pin* and *flipper* are all positioned using a 3-point scheme, using the axis of the spacers as the rotation axis, and a point at the surface of the *shell* as the locker of the Z-translation.

The screws are positioned relative to the parts they link, using a 2-point positioning scheme. Thus, they accumulate the variation errors.

flipper_del is positioned primarily relative to *flipper* and *spacer*15 using a $3-2-1$ positioning scheme. Their main interface is a contact XY-plane between *flipper_del* and *flipper*, and the spacer is its rotation axis.

The variations over the system can be seen in Figure 22.

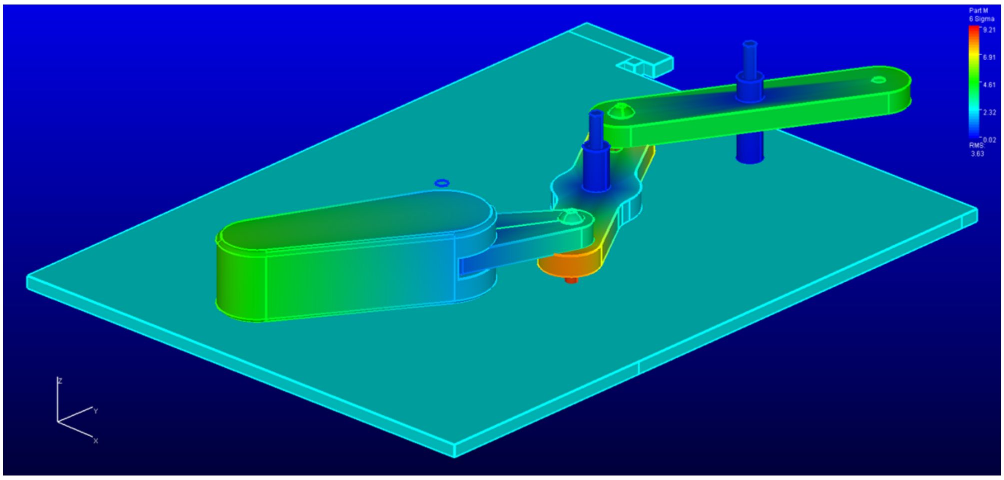

Figure 22: Amplitude of variations across the mechanism by itself, linked to its container (not represented here)

4.2.6 Measures

The sensitivity matrix given by RD&T for all our measures is shown in Figure 23. The orange and green lines correspond to the study of the coaxiality of the transmission axis, while the pink lines correspond to the possible collision between *shell* and *flipper_del*.

Measure (RSS) \ Positioning [RSS]	M3_201	M3_20	M3_15	spacer20	spacer201	spacer15	handle	shell	high_plate	lateral_plate	hex_handle_transferpin	transferpin	flipper	flipperD	hex_transferpin_flipper
Coaxiality_handle_transferpin	0.51	0.51	0.00	1.74	1.71	0.00	4.85	0.00	0.13	0.13	0.00	3.23	0.00	0.00	0.00
Coaxiality_transferpin_flipper	0.00	0.49	5.31	1.72	0.00	0.55	0.00	0.00	0.39	2.04	0.00	3.22	2.54	0.00	0.00
Dist_shell_flipperD1	0.62	0.30	2.08	0.05	0.00	0.02	0.00	29.78	0.29	3.47	0.00	0.57	1.19	6.49	0.00
Dist_shell_flipperD2	0.61	0.25	0.95	0.05	0.00	0.09	0.00	30.57	0.23	3.40	0.00	0.57	1.19	7.14	0.00
meas_axis_transferpin_flipper	0.23	0.30	0.77	1.13	0.00	0.03	0.00	9.49	0.05	0.37	0.00	4.33	0.17	0.00	0.00
meas_axis_transferpin_handle	0.27	0.27	0.00	0.84	1.88	0.00	5.08	17.67	0.06	0.08	0.00	4.59	0.00	0.00	0.00

RMS Tot: 5.29

Figure 23: Impact of the variations of the parts over the measurements

Coaxiality of transmission axis: The measures regarding the coaxiality of the transmission axis have been studied in Section 3.3.

We concluded that the parallelism between the axes was satisfying, but their matching points suffer from too high a distance compared to the actual margin. The suggested solution consists of increasing the functional gap in the tolerance stacking between the diameters, but this would actually have little impact. Indeed, only $handle$, $transfer\_pin$ and $flipper$ were considered in Section 3.3. We did not dwell on the most important variation factor, which is $shell$.

Contact between $flipper\_del$ and $shell$: The aim is to ensure the flipper can actually move up to $30deg$ in spite of variations.

We consider the distance between two pairs of two points. Two points in a pair have the same Z-coordinate. One point is on the edge of $shell_del$ and the other is on the surface of $shell$. Their exact coordinates have been calculated using CATIA V5 to determine the shorter distance segment between the two parts. A pair of points is located at the top of $flipper\_del$ and the other is at its bottom, to enable comparison knowing that the surfaces are not exactly parallel.

In 95% of cases ($\pm 2\sigma$), the distances between the parts are $3.66mm \pm 4.7mm$ and $3.52mm \pm 4.76mm$. Moreover, none of the 1000 simulations using the Monte Carlo method conclude to a value inferior to zero, since the negative variation compared to the mean is strictly superior to 1.5σ. In other words, $flipper\_del$ has very low risks of colliding with $shell$ during its movement.

Unsurprisingly, the measures are mostly influenced by $shell$ variations. Variations over $flipper\_del$ are roughly 5 times less significant.

4.2.7 Suggested mitigations

In all of our measures, the shell is the main contributor to the variations of the system.

It contributes to the positioning of the parts and suffers from high variations due to 3D printing and positioning. Indeed, its $3-2-1$ positioning is firstly based on both axes of $M320$ and $M3201$. Its interface with *low_plate* is only considered as the last point to lock Z-translations, leading to high variations. This is illustrated in Figure 24.

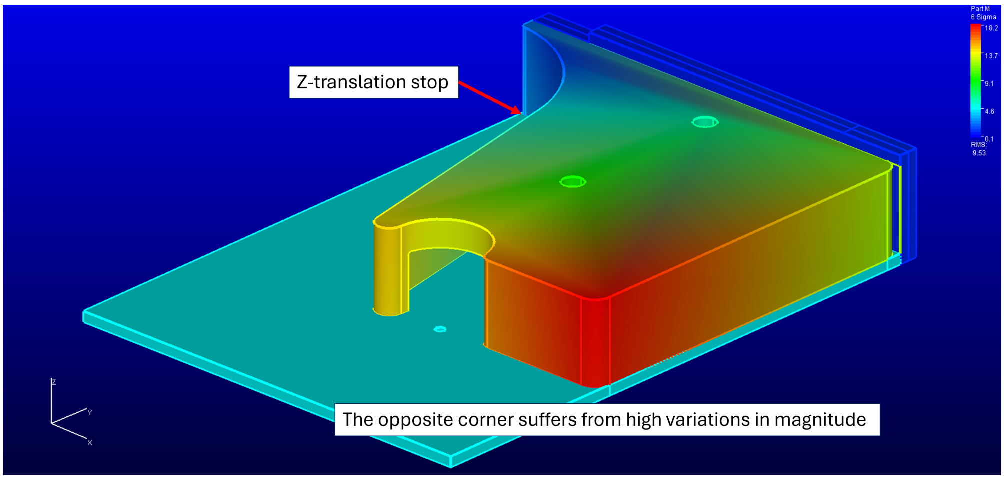

Figure 24: Consequences of the positioning of *shell* relative to *low_plate*

The shell should have two positioning points on its interface with *low_plate* so one hole of $M320$ or $M3201$ should be converted to a slot. Moreover, the shell does not have to adhere to *lateral_plate* and its Y-length could be reduced. In the model, *shell* was positioned relative to the holes in *high_plate*, but in reality, Y-variations could impede this positioning, since its nominal length makes it adhere to *lateral_plate*.

If this solution was not satisfying, we could change the positioning part for screws and spacers. It is difficult to improve the resolution of 3D printing. Nevertheless, laser cutting is more precise. We could have had a second *low_plate* on top of the first one, whose holes had the diameter of the spacers. Thus, the positioning of the screws and the spacers would have relied on laser-cut parts, while the shell would only have had an aesthetic role. Nevertheless, "best part is no part": the positioning of this new part could have also come with uncertainties.